The Astrophysical Journal Letters, 721:L67–L71, 2010 September 20 doi:10.1088/2041-8205/721/1/L67

DETECTING OCEANS ON EXTRASOLAR PLANETS USING THE GLINT EFFECT

Tyler D. Robinson[1,3], Victoria S. Meadows[1,3], and David Crisp[2,3]
[1] Astronomy Department, University of Washington, Seattle, WA 98195, USA; robinson@astro.washington.edu
[2] Jet Propulsion Laboratory, Pasadena, CA 91109, USA
Received 2010 June 22; accepted 2010 August 19; published 2010 September 2

ABSTRACT

Glint, the specular reflection of sunlight off Earth's oceans, may reveal the presence of oceans on an extrasolar planet. As an Earth-like planet nears crescent phases, the size of the ocean glint spot increases relative to the fraction of the illuminated disk, while the reflectivity of this spot increases. Both effects change the planet's visible reflectivity as a function of phase. However, strong forward scattering of radiation by clouds can also produce increases in a planet's reflectivity as it approaches crescent phases, and surface glint can be obscured by Rayleigh scattering and atmospheric absorption. Here, we explore the detectability of glint in the presence of an atmosphere and realistic phase-dependent scattering from oceans and clouds. We use the NASA Astrobiology Institute's Virtual Planetary Laboratory three-dimensional line-by-line, multiple-scattering spectral Earth model to simulate Earth's broadband visible brightness and reflectivity over an orbit. Our validated simulations successfully reproduce phase-dependent Earthshine observations. We find that the glinting Earth can be as much as 100% brighter at crescent phases than simulations that do not include glint, and that the effect is dependent on both orbital inclination and wavelength, where the latter dependence is caused by Rayleigh scattering limiting sensitivity to the surface. We show that this phenomenon may be observable using the *James Webb Space Telescope* paired with an external occulter.

Key words: astrobiology – Earth – planets and satellites: composition – radiative transfer – scattering – techniques: photometric

1. INTRODUCTION

A major goal in the study of extrasolar planets is the detection and recognition of a "habitable" world or a planet capable of maintaining liquid water on its surface. A variety of direct and indirect approaches could be used to determine if a planet is habitable. Indirect approaches focus on characterizing the surface environment of a planet, which would constrain the likelihood that the planet could maintain liquid water on its surface. Direct approaches aim to detect signs that indicate the presence of water on the surface of a planet (e.g., Cowan et al. 2009).

One direct indicator of surface bodies of water is specular reflection or the "glint effect." While specular reflection is not unique to liquid surfaces (e.g., Dumont et al. 2010), liquids are distinguished from other surfaces by their contrast between weak specular reflectance at direct illumination angles and strong specular reflectance at glancing illumination angles. Recently, Stephan et al. (2010) used the enhanced reflectivity of liquids at glancing illumination angles to provide evidence for liquid hydrocarbon lakes on the surface of Titan.

Sagan et al. (1993) argued that the presence of a specularly reflecting region (or "glint spot") in spatially resolved images of Earth taken by the *Galileo* spacecraft, combined with detections of atmospheric water vapor and surface temperatures near the melting point of water, was evidence for the presence of liquid water oceans on Earth's surface. Unfortunately, obtaining spatially resolved images of terrestrial extrasolar planets presents an engineering challenge that will not be met in the near future. The first measurements that aim to detect glint must rely on how it affects the brightness of a planet in a disk-integrated sense.

The relative size of Earth's glint spot compared to the illuminated portion of the disk increases at crescent phases, and the reflectivity of water increases at glancing illumination angles, affecting Earth's phase curve. The detectability of this effect was first investigated by Williams & Gaidos (2008), who used a simple model of Earth's reflectance coupled to a three-dimensional climate model to predict Earth's appearance over the course of an orbit. Their model showed that Earth's reflectivity increases into crescent phases, but was unable to reproduce Earthshine observations of Earth's reflectivity (Pallé et al. 2003). This discrepancy was attributed to the absence of Rayleigh scattering in their model and the assumption that clouds reflect isotropically (Lambertian). In reality, liquid droplets and ice crystals preferentially scatter light in the forward direction, which can mimic the glint effect.

Oakley & Cash (2009) modeled Earth's brightness over the course of an orbit with an emphasis on characterization by the New Worlds Observer mission concept (Cash 2006). Their model simulated Earth's reflectivity using satellite-measured bidirectional reflectance distribution functions (BRDFs) for a variety of scenes (e.g., thick cloud over ocean; Manalo-Smith et al. 1998), and used satellite observations to evolve clouds, snow, and ice in their simulations. Their model also demonstrated an increase in Earth's reflectivity into crescent phases, but was not compared to the phase-dependent Earthshine measurements. The authors proposed that the bright glint spot increases the variability in Earth's brightness at crescent phases, which could serve as an indicator of surface oceans. However, the BRDFs used in their model were not valid at extreme crescent phases, requiring assumptions about cloud scattering and ocean reflectivity at glancing illumination angles.

In this work, we use the NASA Astrobiology Institute's Virtual Planetary Laboratory (NAI-VPL) three-dimensional spectral Earth model to simulate Earth's disk-integrated spectrum as it would appear to a distant observer watching the planet through an orbit. While extensively validated against time-dependent data in Robinson et al. (2010), we present further validations here against phase-dependent Earthshine observations.

[3] NASA Astrobiology Institute

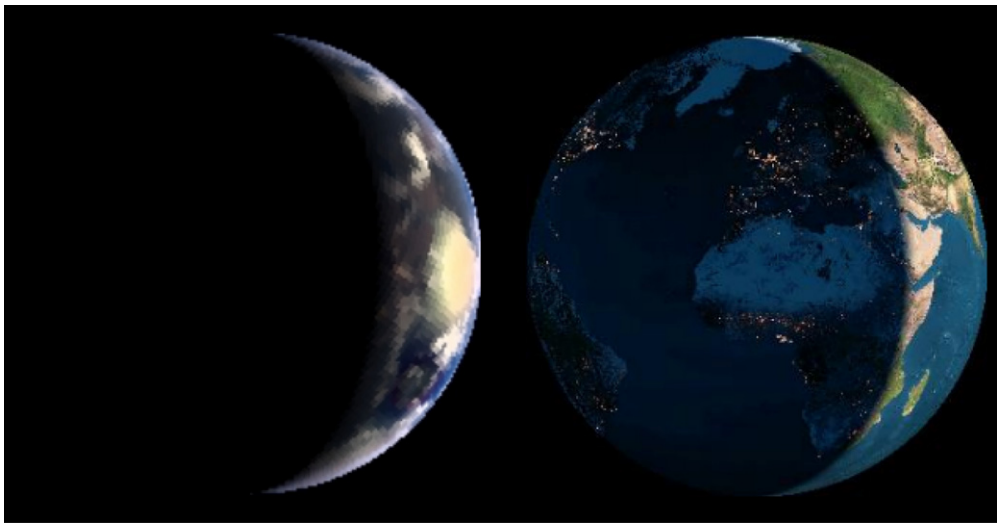

Figure 1. True-color image from our model (left) compared to a view of Earth from the Earth and Moon Viewer (http://www.fourmilab.ch/cgi-bin/Earth/). A glint spot in the Indian Ocean can be clearly seen in the model image.

The validated model is used to investigate the significance of glint in Earth's phase curve by discriminating between the competing effects of cloud scattering and glint. We also discuss the observing requirements for glint detection.

2. MODEL DESCRIPTION

The NAI-VPL three-dimensional spectral Earth model simulates Earth's appearance to a distant observer. The model produces spatially and spectrally resolved datacubes that can be collapsed to produce high-resolution, disk-integrated spectra, and was described and validated in Robinson et al. (2010), so only a brief summary will be presented here. Additional information can be found in Tinetti et al.(2006a, 2006b).

The three-dimensional spectral Earth model simulates Earth's spectrum at arbitrary viewing geometry over wavelengths from the far-ultraviolet to the far-infrared on timescales from minutes to years. Earth-observing satellites provide spatially resolved, date-specific inputs of key surface and atmospheric properties. To simulate the seasonal changes in Earth's appearance over a year, we use snow cover and sea ice data as well as cloud cover and optical thickness data from the Moderate Resolution Imaging Spectroradiometer (MODIS) instruments (Salomonson et al. 1989) aboard NASA's Terra and Aqua satellites (Hall et al. 1995; Riggs et al. 1999).

Specular reflectance from liquid water surfaces in our model is simulated using the Cox–Munk glint model (Cox & Munk 1954), which allows for the calculation of the BRDF of a wave-covered ocean given wind speed and direction, which are provided by the QuikSCAT satellite (http://winds.jpl.nasa.gov/missions/quikscat/index.cfm). Wavelength-dependent optical properties for liquid clouds are derived using a Mie theory model (Crisp 1997) and ice clouds are parameterized using geometric optics (Muinonen et al. 1989). Figure 1 shows a true-color image generated by our model, demonstrating the glint effect and the ability of clouds to mimic this effect.

3. MODEL VALIDATION

Our model was previously validated against time-dependent ultraviolet through mid-infrared observations (Robinson et al. 2010), but for a narrow range of phases. Here, we extended our validation by matching Earthshine measurements of Earth's apparent albedo at a variety of phases between gibbous and crescent (Pallé et al. 2003). The apparent albedo is defined as the albedo of a perfect Lambert sphere that would give the same reflectivity of a body at a given phase angle. Thus, the apparent albedo of a Lambert sphere would be constant through all phases.

Figure 2 shows our simulation of Earth's brightness and corresponding apparent albedo as it would appear over the course of one year to a distant observer (black curves). Observations from NASA's *EPOXI* mission (Livengood et al. 2008) as well as a large number of ground-based Earthshine observations are also shown. Observations and model results span the wavelength range 0.4–0.7 μm. *EPOXI* observations were recorded over three separate 24 hr periods in March, May, and June of 2008, while Earthshine measurements span 1998 November through 2005 January. Calibration errors as large as 10% are present in the *EPOXI* observations (Klaasen et al. 2008) while Earthshine observations have a stated accuracy of 2% (Qiu et al. 2003).

In general, there is good agreement between the data and the model, demonstrating the ability of the model to properly simulate Earth's phase-dependent brightness. At gibbous phases where Earthshine data were recorded, the mean apparent albedo of the model Earth is 0.29 ± 0.02 and is 0.26 ± 0.03 for the Earthshine data. Thus, while the Earthshine data are systematically lower than the *EPOXI* observations and the model at gibbous phases, they are all in agreement to within one standard deviation. At crescent phases, the Earthshine observations are systematically larger than the model. However, an analysis where the Earthshine data were divided into 10° wide bins in orbital longitude shows that the model is always within a single standard deviation of the observations.

4. RESULTS

In the subpanel of Figure 2, the glinting model demonstrates an excess in brightness as large as 50% over the non-glinting model (gray curves), which uses an isotropically scattering ocean reflectance model whose albedo reproduces Earth's geometric albedo to within a few percent. The excess brightness increases into crescent phases as the contribution of the glint spot to Earth's disk-integrated brightness grows, peaking at

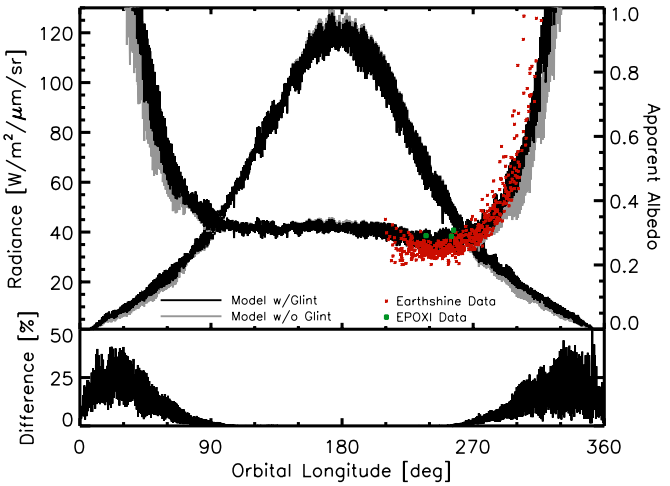

Figure 2. Simulation of Earth through a year. The black line corresponds to a model that includes glint while the gray line corresponds to a model that does not include glint. The left *y*-axis corresponds to the bell-shaped curves, demonstrating that Earth is brightest at full phase (orbital longitudes near 180°) and faintest near crescent phase (orbital longitudes near 0° and 360°). The right *y*-axis corresponds to the bowl-shaped curves, where a perfect Lambert sphere would have a constant apparent albedo with phase. Variability at small timescales is due to Earth's rotation and time-varying cloud formations (noise is not included in simulations). Model "observations" are recorded every four hours, the system is viewed edge-on ($i = 90°$), and an orbital longitude of 0° corresponds to 2008 January 1. Small stars are Earthshine measurements of Earth's apparent albedo (Pallé et al. 2003). Large circles are 24 hr average measurements of Earth's apparent albedo recorded by the Deep Impact flyby spacecraft as part of NASA's *EPOXI* mission (Livengood et al. 2008). All data and model observations span the wavelength range 0.4–0.7 μm. The bottom sub-panel demonstrates the brightness excess seen in the glinting model over the non-glinting model.

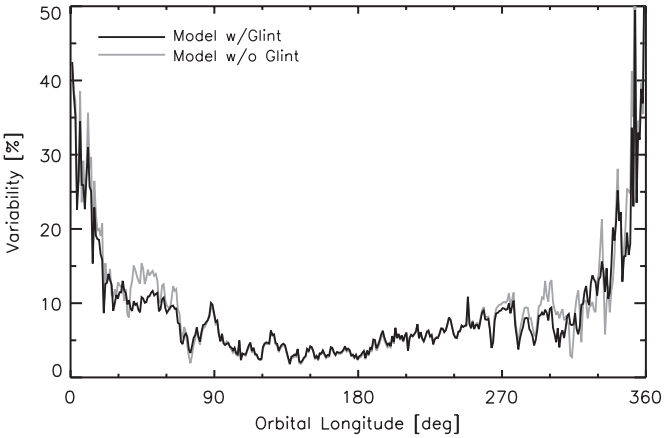

Figure 3. Variability in brightness for our glinting model (black) and our non-glinting model (gray), which are both shown in Figure 2. Details are discussed in the text.

orbital longitudes near 20°–30° from new phase. The brightness excess declines as the illuminated crescent shrinks further. This is due to a wave-surface "hiding" effect discussed in Cox & Munk (1954), where ocean waves block rays of light at glancing illumination angles.

The brightness difference between the glinting and non-glinting model is a strong function of wavelength. If we instead choose a filter that spans 1.0–1.1 μm, the peak brightness excess increases to about 100%. This behavior arises because glint occurs at the surface and some wavelength ranges are more sensitive to Earth's surface than others.

Near 90° orbital longitude, both models in Figure 2 have apparent albedos that are about 15%–20% larger than those near 270°. This is due to Earth's seasons, as was noted in Williams & Gaidos (2008), and was determined by comparing to a model run without any seasonal evolution of snow and ice. As Earth moves from northern winter to northern summer (0° to 180° orbital longitude in these simulations, respectively), the illumination of the northern polar region, which is tilted toward the observer, increases. Since this region of Earth is more snow and ice covered prior to northern summer than following northern summer, the planet appears more reflective heading into full phase than moving out of full phase. The magnitude of this asymmetry in the light curve agrees with the simulations of Oakley & Cash (2009). In general, the effects of seasons on Earth's light curve depend on viewing geometry, but are small compared to the effects of cloud scattering and glint at crescent phases.

The variability of both models in Figure 2, defined as the ratio between the standard deviation of all model observations from a 24 hr period and the 24 hr average brightness from the same timespan, is shown in Figure 3. The variability steadily increases from about 5% near full phase to about 30%–40% near crescent phase. Brightness is more variable at crescent phases since the illuminated portion of the disk represents a relatively small fraction of the planet's surface area and, thus, is easily dominated by clouds that rotate into view or a cloud-free view of the glint spot. Variability at gibbous phases following northern summer is slightly larger than variability at gibbous phases prior to northern summer (4% versus 6%, respectively), which is a seasonal effect. The magnitude of the variability in our models agrees well with the simulations of Oakley & Cash (2009). However, these authors did not find a seasonal dependence in variability measurements. Furthermore, their simulations show a sharp increase in variability as the planet moves into crescent phases (variability increases from 5%–10% to 40% over about 10° of orbital longitude) while our models show a gradual increase in variability into crescent phases.

5. DISCUSSION AND CONCLUSIONS

5.1. Earth with and without Glint

Including phase-dependent reflection from oceans and clouds as well as Rayleigh scattering has allowed us to reproduce both the brightness and phase dependence of Earthshine observations. Williams & Gaidos (2008) explicitly ignored Rayleigh scattering and phase-dependent scattering from clouds and were unable to reproduce Earthshine observations, demonstrating the importance of including these effects in a realistic spectral Earth model. A model that only includes phase-dependent Rayleigh scattering produces an increase in apparent albedo at crescent phases (due to weak forward and backward scattering lobes in the Rayleigh scattering phase function), but the upturn occurs only at extreme crescent phases (at orbital longitudes within 30° of new phase), which is not seen in Earthshine observations. This argues that the lack of phase-dependent cloud scattering in the model presented in Williams & Gaidos (2008) was the primary reason why their model could not reproduce Earthshine observations. Thus, predictions regarding the behavior of Earth's brightness at crescent phases are especially reliant on realistic cloud modeling.

Models that do not include the "hiding" effect of ocean waves will overestimate the brightness of water surfaces at glancing

reflection angles. For edge-on orbits (inclination, $i = 90°$), this effect becomes especially important at orbital longitudes within about 30° of new phase, in agreement with Cox & Munk (1954). The phase-dependent relative size of the glint spot, the tendency of water to be more reflective at glancing reflection angles, and the "hiding" effect all combine to produce a maximum brightness excess for a realistic Earth over an Earth without glint near 30° from new phase (for an orbit viewed edge-on). Varying ocean wind speeds in our model show that the location of this peak is only weakly dependent on surface wind conditions. Previous models used to investigate the detection of surface oceans (Williams & Gaidos 2008; Oakley & Cash 2009) do not include the "hiding" effect and cannot make strong statements about glint detection at extreme crescent phases.

The season- and phase-dependent variability of Earth's brightness, shown in Figure 3 and taken from the edge-on simulations shown in Figure 2, is due to contrast between highly reflective surfaces and surfaces with low reflectivity. Following full phase, which corresponds to northern summer in our simulations, snow and sea ice in the northern polar region have been replaced by darker surfaces (e.g., grassland) which provide greater contrast to clouds as compared to the snow and ice present prior to full phase. Thus, variability is larger following northern summer in our simulations. At crescent phases, contrast is provided by bright, forward-scattering clouds, and/or the bright glint spot, against relatively dark, Lambertian-scattering surfaces. The illuminated sliver of the planet at crescent phases represents a relatively small amount of surface area so that the illuminated disk at these phases can become dominated by large cloud features (or the glint spot), leading to large variability. Near full phase, the illuminated disk represents a large amount of surface area, averaging over clouded and non-clouded scenes, leading to relatively low variability.

Our simulations without glint produce the same rise in variability into crescent phases as our simulations with glint, which indicates that variability at crescent phases is not completely driven by glint. Thus, the trend of increasing variability into crescent phases is not a clear indicator of surface oceans, as was proposed by Oakley & Cash (2009). Any planet that can achieve sufficient contrast between bright and dark surfaces will produce a variability signal that increases into crescent phases, regardless of the presence of oceans.

Our glinting model demonstrates a wavelength-dependent brightness excess over our non-glinting model, since some wavelengths are more sensitive to surface effects than others. The excess shrinks to less than 10% for the wavelength range 0.3–0.4 μm, where Rayleigh scattering obscures the surface. At wavelengths that correspond to relatively deep absorption bands, like the 1.4 μm water band, the excess shrinks to nearly zero because observations are mostly insensitive to the surface.

At crescent phases, pathlengths through the atmosphere are relatively large and optical depths to Rayleigh scattering can be larger than unity even at longer wavelengths. This indicates that observations which aim to detect the brightness excess due to glint should be made at wavelengths in the near-infrared range. Earth's brightness drops by over an order of magnitude between 1 and 2 μm, arguing that searches for glint should occur below 2 μm for higher signal-to-noise ratio (S/N) detections. Since glint is a broad feature in wavelength space (it is the reflected solar spectrum, modulated by Rayleigh scattering, liquid water absorption at the surface, and atmospheric absorption), photometry can be used to detect glint provided that strong absorption features are avoided.

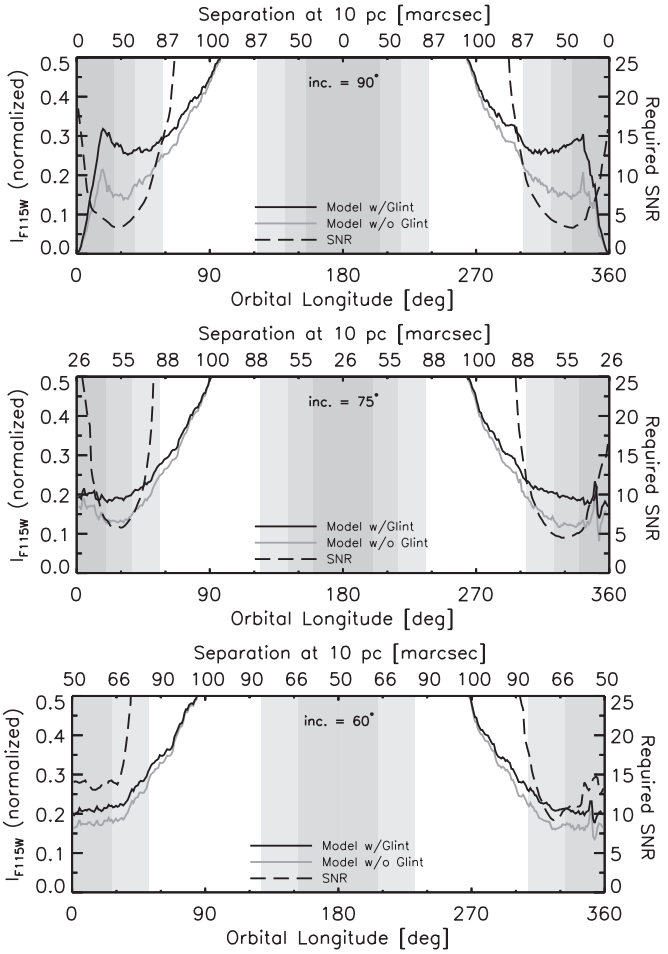

Figure 4. Earth's brightness through the *JWST*/NIRCam F115W filter (spanning 1.0–1.3 μm) relative to its brightness at gibbous phase (135° and 225° orbital longitude) for orbital inclinations of 90° (top), 75° (middle), and 60° (bottom). The glinting model is in black and the non-glinting model is in gray. Vertical shaded regions indicate the portions of the orbit for which a planet orbiting at 1 AU from its host star is within 85 mas, which is a standard IWA for an occulter paired with *JWST* (Brown & Soummer 2010), for a system at a distance of 5 pc (darkest), 7.5 pc (medium), and 10 pc (lightest). Planet–star separation at a distance of 10 pc is shown on the upper *x*-axis. The S/N required to distinguish the glinting model from the non-glinting model at the 1σ level is shown along the right *y*-axis and corresponds to the dashed line. Observations have been averaged over 24 hr periods.

5.2. Observing Requirements for Glint Detection

The glint effect is strongest at NIR wavelengths, so that pairing *James Webb Space Telescope* (*JWST*; Gardner et al. 2006) with an external occulter (e.g., Soummer et al. 2009; Cash 2006) would present a near-term opportunity for the detection of oceans on extrasolar planets. Here, we discuss optimal filter selection and inner working angle (IWA) and S/N requirements for glint detection at wavelengths accessible to *JWST*.

The *JWST* Near Infrared Camera (NIRCam; Horner & Rieke 2004) offers several medium and wide band filters suitable for glint detection, with the F115W, F150W, and F162M filters (spanning 1.0–1.3 μm, 1.3–1.7 μm, and 1.55–1.70 μm, respectively) being most ideal. The F115W and F150W filters partially overlap water absorption features but experience a photon flux 3–4 times larger than the F162M filter, which does not span any strong water features and, thus, has an increased sensitivity to surface effects.

Figure 4 demonstrates a strategy that could be used to observe the brightness excess from glint. We show the 24 hr average brightness of Earth through the F115W NIRCam filter normalized to an observation at gibbous phase for several different orbital inclinations. Also shown is the S/N required to distinguish our glinting model from our non-glinting model at the 1σ level assuming that high-S/N observations (S/N = 20) have been made at gibbous phase. For the inclination equals 90° and 75° cases, the glinting model shows a distinct leveling-off of its normalized brightness at crescent phases. Relative to its brightness at gibbous phase, the planet's brightness can remain roughly constant through certain phases due to the competing effects of the falling stellar illumination and the rising reflectivity due to glint. The glint effect becomes difficult to detect for the case where inclination equals 60° because the planet never becomes a small enough crescent to produce a strong glint effect. Minimum S/Ns between 5 and 10 are required for glint detection, depending on viewing geometry and telescope IWA. Note that roughly 25% of all planets discovered will have orbital inclinations between 75° and 105° and 50% will have inclinations between 60° and 120°.

Observations of Earth-like exoplanets at crescent phases can be difficult due to IWA constraints. Vertical shaded regions in Figure 4 represent portions of the planet's orbit that cannot be observed for an Earth twin at different distances assuming an IWA of 85 mas (Brown & Soummer 2010), demonstrating that the glint effect could be detected for near edge-on orbits out to a distance of about 8 pc for this IWA. The measure of planet–star separation shown along the top of the sub-figures indicates that an IWA of about 50 mas would allow for the easiest detection of the glint effect for planets within 10 pc. Note that angular separation will scale inversely with distance to the system, and that the IWA constraints become significantly less strict for an Earth-like planet at the outer edge of the Habitable Zone.

6. CONCLUSION

Our model successfully reproduces Earth's phase-dependent brightness from Earthshine observations. We have shown that glint increases Earth's brightness by as much as 100% at crescent phases, and that this effect is strongest in wavelength regions that are unaffected by Rayleigh scattering and atmospheric absorption. The glint effect may be detectable using *JWST*/NIRCam paired with an external occulter. Depending on viewing geometry, minimum S/Ns of 5–10 are required for glint detection and an optimal IWA for detection is about 50 mas for an Earth twin at 10 pc.

This work was performed by the NASA Astrobiology Institute's Virtual Planetary Laboratory, supported under solicitation no. NNH05ZDA001C.

REFERENCES

Brown, R. A., & Soummer, R. 2010, ApJ, 715, 122
Cash, W. 2006, Nature, 442, 51
Cowan, N. B., et al. 2009, ApJ, 700, 915
Cox, C., & Munk, W. 1954, J. Opt. Soc. Am., 44, 838
Crisp, D. 1997, Geophys. Res. Lett., 24, 571
Dumont, M., Brissaud, O., Picard, G., Schmitt, B., Gallet, J., & Arnaud, Y. 2010, Atmos. Chem. Phys., 10, 2507
Gardner, J. P., et al. 2006, Space Sci. Rev., 123, 485
Hall, D. K., Riggs, G., & Salomonson, V. V. 1995, Remote Sens. Environ., 54, 127
Horner, S. D., & Rieke, M. J. 2004, Proc. SPIE, 5487, 628
Klaasen, K. P., et al. 2008, Rev. Sci. Instrum., 79, 091301
Livengood, T. A., et al. 2008, BAAS, 40, 385
Manalo-Smith, N., Smith, G. L., Tiwari, S. N., & Staylor, W. F. 1998, J. Geophys. Res., 103, 19733
Muinonen, K., Lumme, K., Peltoniemi, J., & Irvine, W. M. 1989, Appl. Opt., 28, 3051
Oakley, P. H. H., & Cash, W. 2009, ApJ, 700, 1428
Pallé, E., et al. 2003, J. Geophys. Res. (Atmos.), 108, 4710
Qiu, J., et al. 2003, J. Geophys. Res. (Atmos.), 108, 4709
Riggs, G., Hall, D. K., & Ackerman, S. A. 1999, Remote Sens. Environ., 68, 152
Robinson, T. D., et al. 2010, Icarus, submitted
Sagan, C., Thompson, W. R., Carlson, R., Gurnett, D., & Hord, C. 1993, Nature, 365, 715
Salomonson, V. V., Barnes, W. L., Maymon, P. W., Montgomery, H. E., & Ostrow, H. 1989, IEEE Trans. Geosci. Remote Sens., 27, 145
Soummer, R., et al. 2009, Proc. SPIE, 7440, 74400A-1
Stephan, K., et al. 2010, Geophys. Res. Lett., 37, 7104
Tinetti, G., Meadows, V. S., Crisp, D., Fong, W., Fishbein, E., Turnbull, M., & Bibring, J.-P. 2006a, Astrobiology, 6, 34
Tinetti, G., Meadows, V. S., Crisp, D., Kiang, N. Y., Kahn, B. H., Fishbein, E., Velusamy, T., & Turnbull, M. 2006b, Astrobiology, 6, 881
Williams, D. M., & Gaidos, E. 2008, Icarus, 195, 927